



Computational modelling and experimental validation of pressure drop through multi-layered woven screens for polymer melts

Joseph D. Bennett^{a,*}, Mark C.T. Wilson^b, Nikil Kapur^b, Peter K. Jimack^c, Richard P. Maltby^d, M. Kieran Looney^d

^a EPSRC CDT in Fluid Dynamics, University of Leeds, LS2 9JT, UK

^b School of Mechanical Engineering, University of Leeds, LS2 9JT, UK

^c School of Computing, University of Leeds, LS2 9JT, UK

^d Mylar Specialty Films UK Limited, The Wilton Centre, Redcar, TS10 4RF, UK

ARTICLE INFO

Dataset link: [10.17632/md487w94k2.1](https://doi.org/10.17632/md487w94k2.1)

Keywords:

Polymer melt processes

Screen filters

Porous media modelling

Computational fluid dynamics

ABSTRACT

Woven screens are commonly used in filtration processes that involve molten polymer. Predicting the initial pressure drop across these screens is crucial for selecting an appropriate filtration system as it directly affects the efficiency and cost-effectiveness in industrial processes. Existing computational models for predicting pressure drop through woven screens have not been developed for multi-layered configurations. This study develops an accurate and reliable methodology for using computational fluid dynamics (CFD) to model the pressure drop across a multi-layered screen. The computational model is validated through an experimental set-up.

1. Introduction

Woven wire meshes are used in many processes in industry (Abou-Hweij and Azizi, 2020; Kołodziej et al., 2009; Laws and Livesey, 1978), including in polymer melt processes as filtration material (Pachner et al., 2017, 2019). Woven screens are extensively used in filtration processes as they offer precise filtration, high filtration efficiency, mechanical strength and thermal resistance (Onufrena et al., 2021; Ali, 2013). These qualities make woven screens particularly advantageous for processes with demanding conditions, such as those encountered in melt filtration.

Mylar Specialty Films produce polyester films on a commercial scale. Polymer chip is extruded into a melt, then converted into a cast sheet through a die (Champion, 2015). The cast sheet is drawn in the machine direction and transverse direction to prepare films with thicknesses between 0.6 and 350 μm (Herman, 2004). A filter sits between the extruder and die, and is tasked with removing any unmelted or degraded material and contaminants, which lead to defects in the cast film and splitting of the film during stretching (Stratiychuk-Dear, 2018). The shear imposed by the filter also improves homogeneity (Pachner et al., 2019). Screen filters often employ multiple screens where, typically, the fine filter layer is supported by stronger, coarser layers (Pachner et al., 2019).

Polyethylene terephthalate (PET) is one of the main polymers used in film production by Mylar Specialty Films (Champion, 2015). Polymer

melts are viscoelastic materials, and are classified as non-Newtonian, shear thinning fluids (Denn, 2008). However, at shear rates imposed in the film production process, PET polymers may be considered Newtonian and inelastic (Champion et al., 2015).

The thermoplastic industry is expected to be valued at more than 500 billion dollars by 2033 (P&S Intelligence, 2024). PET is the most commonly used thermoplastic polymer resin, with a global demand of 42 million metric tons expected by 2030 (Statista, 2024). PET accounts for 7% of the total plastic market (P&S Intelligence, 2024). PET processing is used for manufacturing in industries such as packaging, textiles, electrical and electronics, the automotive industry and many more (Omnexus, 2024). As PET is a thermoplastic, it is easily processed by extrusion and is generally used to produce film and sheets (Omnexus, 2024).

Around 25.8 million tons of plastic waste was generated in the EU in 2019, and the European Strategy for Plastics in a Circular Economy proposed the goal that 75% of packaging waste would be recycled by 2030 (Pachner et al., 2019). Recycled polymer contains high levels of contaminants, which, if not removed, can downgrade the quality of the final product in processing (Pachner et al., 2019). As industry tries to maximize the amount of recycled polymer used in processing to achieve ambitious recycling goals, melt filtration is crucial as it ensures the final product is suitably clean and free of contaminants (Pachner et al.,

* Corresponding author.

E-mail address: mm16j2b@leeds.ac.uk (J.D. Bennett).

<https://doi.org/10.1016/j.cherd.2024.08.002>

Received 8 February 2024; Received in revised form 12 July 2024; Accepted 2 August 2024

Available online 6 August 2024

0263-8762/© 2024 The Author(s). Published by Elsevier Ltd on behalf of Institution of Chemical Engineers. This is an open access article under the CC BY license (<http://creativecommons.org/licenses/by/4.0/>).

Nomenclature

S	Source term, N/m ³
u	Fluid velocity, m/s
x	Position, m
$\Delta\xi$	Corrected pressure drop, psi/Pa s
ΔP	Pressure drop, Pa
\dot{m}	Mass flow rate, kg/hr
μ	Viscosity, Pa s
ρ	Density, kg/m ³
ξ	Corrected pressure, psi/Pa s
A	Cross-sectional area, m ²
C	Forchheimer coefficient
D	Pipe diameter, m
d	Screen thickness, μm
k	Permeability, m ²
P	Pressure, Pa
T	Temperature, °C
t	Time, s
X_D	Development length, m
Re	Reynolds number

2017). Screen filters are widely used for melt filtration and usually consist of multi-layered woven screens (Pachner et al., 2019).

When employing screens in industry, the pressure drop caused by the fluid passing through the screens must be considered. Pressure drop directly affects the cost of the operation, thus must be balanced to achieve optimal efficiency and cost-effectiveness in industrial processes (Azizi, 2019). Pressure drop can impact various aspects of the operation, including energy consumption, pump requirements, maintenance frequency and overall process performance. The initial pressure drop of the system must be determined for selection of a suitable filtration system (Pachner et al., 2019).

Pressure drop through a porous medium may be described by the Forchheimer equation, given by

$$\Delta P = (\mu/k)u + 0.5Cu^2, \quad (1)$$

where ΔP is the pressure drop across the porous medium, μ is the viscosity of the fluid, k is the permeability of the porous medium, ρ is the density of the fluid, u is the velocity of the fluid and C is the Forchheimer coefficient. When the Reynolds number is less than one, inertial effects can be ignored and Darcy's law applies (Sidiropoulou et al., 2007), reducing (1) to

$$\Delta P = (\mu/k)u. \quad (2)$$

Modelling pressure drop through a woven screen has been the subject of analytical (Azizi, 2019; Wang et al., 2021; Carley and Smith, 1978), experimental (Kołodziej et al., 2009; Yangpeng et al., 2015) and computational (Valli et al., 2009; Teitel, 2011, 2010) research due to the prevalence of screens in industrial processes such as melt filtration. Other applications in industry include, but are not limited to: static mixers to superimpose turbulence (Abou-Hweij and Azizi, 2020), catalyst reactors as catalyst support material (Kołodziej et al., 2009) and wind tunnels for the dissipation or generation of flow non-uniformities (Laws and Livesey, 1978).

The flow profile in a pipe upstream, downstream and through a structured woven mesh with uniformly distributed pores and pore sizes was computationally investigated by Abou-Hweij and Azizi (2020). As the flow approaches a screen, the resistance caused by its presence flattens the fully developed parabolic velocity profile. As the flow passes through the screen, all the fluid passes through screen openings, leading to high velocity jets through the openings and zero flow

where screen wires exist. The flattening effect on the velocity profile is more pronounced with decreasing screen permeability (Abou-Hweij and Azizi, 2020).

In CFD, when modelling porous media, it may be computationally expensive to refine a mesh at the scales of pores while modelling the entirety of the porous medium and surrounding geometry (Teitel, 2010). To this end, macroscopic models are used. A popular model used in CFD is the porous media model (ANSYS, 2012b), which prescribes some properties to a cell zone in the computational geometry, known as a porous zone, imposing a pressure penalty through it.

The porous media model has been used to predict pressure drop through porous media in a range of flow applications. Pashchenko et al. (2020) determined the pressure drop characteristics for fixed bed reactors filled with porous particles using a porous zone with an average error of less than 10%. Cornejo et al. (2019) computationally modelled the pressure drop through a monolith using a multi-zone model. Multiple porous zones were employed to account for entering, passing through and leaving the substrate. This was observed to improve accuracy of the total pressure drop across the monolith compared to prior models.

Porous zones have been used to model pressure drop across woven screens. Teitel (2010) found that the pressure drop through a screen can be determined by the porous media model, reducing computational time significantly as there was no need to refine the mesh to resolve flow near screen wires. Teitel (2011) used a porous zone to represent a woven screen to investigate if the Forchheimer coefficient is constant over a wide range of Reynolds numbers. Garg et al. (2019) modelled a stacked woven wire mesh with a porous zone in a miniature Stirling cryocooler, with the goal of capturing accurate heat transfer characteristics. In the porous medium, a local thermal equilibrium model and local thermal non-equilibrium model were used to model the energy equation in the porous zone; the non-equilibrium model was shown to give better understanding of the heat transfer characteristics in the stacked wire mesh. Trilok et al. (2022) used a porous zone to model the pressure drop through stacked woven wire mesh for heat exchange applications; pressure drop across the stacked mesh was in good agreement with an experiment, with an average discrepancy of less than 8%.

While CFD models employing porous zones have been developed to predict pressure drop through single-layer woven screens (Teitel, 2010, 2011) or, more recently, stacked woven wire meshes (Trilok et al., 2022; Garg et al., 2019), their use in the modelling of multi-layered configurations, where each layer varies in structure and permeability, have not been addressed in existing literature. This study addresses this gap in the literature by testing multiple porous zone configurations against experimental results to define a methodology for utilizing the porous media model to model pressure drop through multi-layered woven screens. By considering the influence of multiple layers on flow behaviour, the developed computational methodology aims to provide a more accurate prediction of pressure drop in practical industrial scenarios while allowing insight into how flow patterns are influenced by screen filter choice in filter systems. We emphasize that the methodology developed in this work is directly applicable to an extensive range of flow systems that utilize multi-layered woven screens.

2. Materials and methods

2.1. Screen filter geometry

In-line screen filters are employed on a pilot-scale film line. An in-line screen filter is shown in Fig. 1b; they are circular structures where filter medium is sandwiched between coarse upstream and downstream support mesh. The filter is inserted into the circular pipe, supported by a filter holder, so that fluid passes through its flat surface. After passing through the filter, the fluid passes through the holder, shown in Fig. 1c, via the circular holes in it.

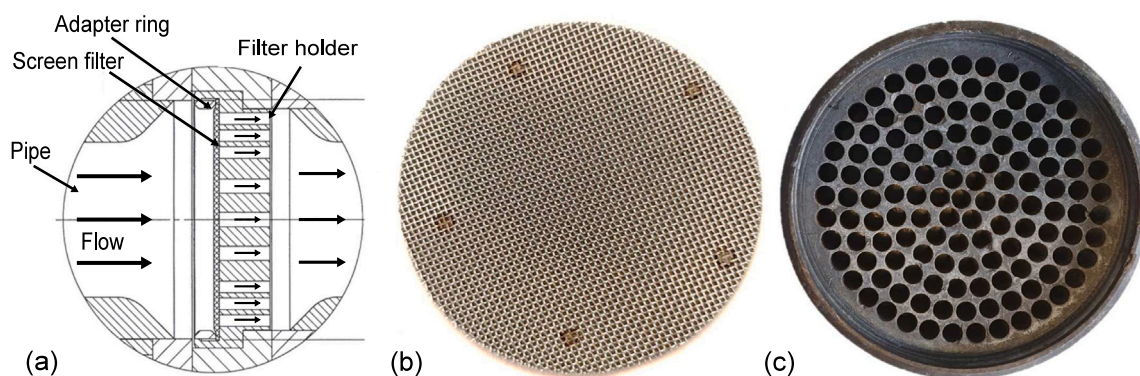


Fig. 1. (a) A cross-section of the geometry around the filter. The adapter ring was not used in the experiment. (b) An in-line screen filter. (c) A filter holder.

This geometrical set-up is shown in Fig. 1a. Melt enters through a circular pipe, which widens in the upstream section prior to encountering the filter. It then traverses the filter and the holder, then, downstream of the holder, the pipe channel constricts to its original diameter. Note that Fig. 1a shows only the geometry in the vicinity of the filter and holder. The pipes in and out of this section extend and remain straight with constant diameter for at least a metre in both directions away from the filter and holder. This ensures fully developed pipe flow upstream and downstream of the filter geometry.

The filter holder is used to keep the in-line filter in place and support it against the high pressures in the extrusion system. The filter sits in the holder, against the surface shown in Fig. 1c. The holder is the only part of the geometry which cannot be modelled as axisymmetric, due to the holes in it.

To understand how permeability influences pressure drop, four grades of filters are utilized during this work. Three-layered 80, 60 and 40 μm filters and a five-layered 23 μm filter. An 80 μm filter captures 99% of particles with diameter larger than 80 μm . The three-layered filters are made up of a downstream support mesh, a filter layer and an upstream support layer. The 23 μm filter is made up of five layers; the filter layer is supported by two upstream support layers and two downstream support layers, for extra mechanical support.

The total thickness of each filter and each support layer was found using a caliper with precision of 10 μm . Each individual layer for each filter was measured three times, as well as the total thickness of each filter. For each filter, the sum of the average measurements of each layer were found to be the same as the average thickness of the filter. Multiple new filters of each grade were available for measurements. Filter layers were able to be separated for individual measurements.

2.2. Experimental set-up

The objective of this experiment was to investigate how pressure drop across an in-line screen filter is influenced by varying throughput and filter permeability. To this end, polymer melt was extruded and pumped through an in-line filter. The throughput and filter were varied throughout and pressure upstream of the filter was recorded. Fig. 2 shows the geometry of the pilot scale extrusion system used for this experiment. PET chip was fed into the extruder via a cold feedstock where it was extruded and maintained at 275 $^{\circ}\text{C}$ by a series of heaters along the extruder, melt system and die. The extrusion system was heated to control viscosity and prevent solidification. A full vacuum was used on the extruder to remove moisture and minimize trapped air in the melt. The polymer melt then passed through the filter holder and then the die.

Initially, no filter was placed within the filter holder. The process then began, where the throughput was gradually increased to flush out any debris from previous use. The experiment proceeded as follows:

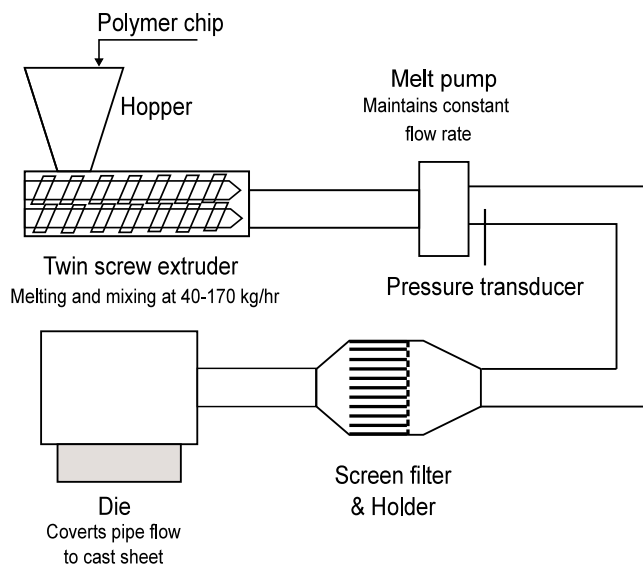


Fig. 2. Sketch of the pilot scale extrusion system.

1. With no filter, the throughput was maintained for at least 15 min at 40, 60, 80, 120 and 160 kg/hr.
2. The throughput was then reduced to 0 kg/hr, the system shut down and an 80 μm screen filter was inserted.
3. The system restarted, and the throughput was maintained at 40, 60 and 80 kg/hr with the 80 μm filter inserted.
4. Steps 2–3 were then repeated with a 60 μm filter.
5. Step 2 was then repeated with a 40 μm filter. The throughput was maintained at 40, 60, 80, 100, 120 and 140 kg/hr in this case.
6. Steps 2–3 were then repeated with a 23 μm filter. The experiment was then concluded and the system was shut down.

Throughput and pressure data were logged every minute. Throughputs were targeted by specifying the rpm of the melt pump. This led to some fluctuations from targeted throughputs. To minimize the impact of any fluctuations, targeted throughputs were maintained for 15 min, and the actual throughput and pressure data was averaged over the final 10 min. Throughputs were maintained in increments of at least 20 kg/hr to maximize the range of data covered. Different throughputs for each filter were chosen to maximize the amount of data recovered over the limited time allowed.

A Minolta/Land Cyclops 79 pyrometer was used to record the temperature of the melt curtain as it fell from the die. This was done for each filter at each maintained throughput to check the temperature of the melt.

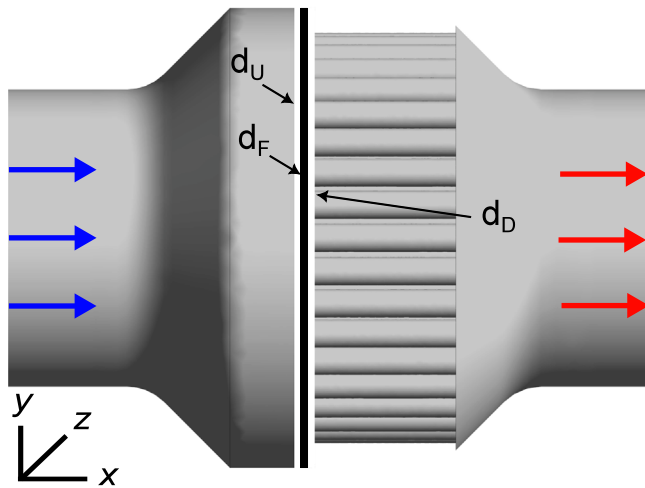


Fig. 3. The virtual geometry used to model flow through a screen filter. The blue and red arrows indicate the flow upstream and downstream of the filter respectively. Note that the figure does not show the whole length of the inlet and outlet pipes. (For interpretation of the references to colour in this figure legend, the reader is referred to the web version of this article.)

2.3. Computational model

Fig. 3 shows the model of the 3D geometry used for CFD simulations. It was created in SOLIDWORKS 2019 using CAD drawings of the pilot line. All simulations were implemented in ANSYS Fluent 2022 R1. At the inlet, a mass flow inlet boundary condition was specified normal to the boundary with a throughput ranging from 40–160 kg/hr. A static pressure outlet boundary condition was chosen with 0 Pa gauge pressure; the inlet and outlet were chosen to be sufficiently far away from the filter and filter holder, as to have no influence on flow development near the filter. All other external boundaries are walls with the no-slip condition applied. An incompressible, Newtonian fluid with $\rho = 1225 \text{ kg/m}^3$ and a viscosity ranging from 120–180 Pa s was

modelled. This puts an upper limit of 0.01 on the Reynolds number, ensuring the laminar regime is maintained throughout.

A steady, pressure-based solver was specified and a viscous, incompressible laminar model was used, that is, the Navier–Stokes equations are discretized and solved using the finite volume method. The Navier–Stokes equations for a viscous, Newtonian fluid are given by

$$\nabla \cdot \mathbf{u} = 0, \tag{3}$$

$$\rho \left(\frac{\partial \mathbf{u}}{\partial t} + \mathbf{u} \cdot \nabla \mathbf{u} \right) = -\nabla P + \mu \nabla^2 \mathbf{u}.$$

A coupled pressure–velocity scheme was used, with least squares cell-based gradient discretization. Second order pressure and second order upwind momentum discretization were also specified. A hybrid initialization method was used. The convergence criterion was set for a maximum scaled residuals of the order 10^{-5} . Furthermore, pressure drop across the geometry and mass imbalance between the inlet and outlet were ensured to vary by less than 0.001% per iteration.

The porous media model (ANSYS, 2012b) was used to represent the screen filter in this model. The porous media model assigns an additional source term in any cell zone where it is enabled, such that

$$\rho \left(\frac{\partial \mathbf{u}}{\partial t} + \mathbf{u} \cdot \nabla \mathbf{u} \right) = -\nabla P + \mu \nabla^2 \mathbf{u} + \mathbf{S}. \tag{4}$$

This source term accounts for the additional pressure drop due to the resistance imposed on the flow by the porous medium and is given by

$$\mathbf{S} = -((\mu/k)\mathbf{u} + 0.5C\rho|\mathbf{u}|\mathbf{u}). \tag{5}$$

Note that the source term is in the form of the Forchheimer Eq. (1). The Forchheimer coefficient is usually determined through empirical relations and $C = 0$ if Darcy’s law applies. The cell zone with the porous media model enabled is known as a porous zone.

In total, twelve variations of the virtual geometry in Fig. 3 were generated to account for varying filter thickness and porous zone position. Permeability inputted into the porous media model is determined based on experimental results. Permeability therefore varied based on filter grade and porous media model configuration. The different porous media model configurations, and their associated permeability values, are discussed in Section 3.2.

A mesh independence study was performed on each mesh to ensure that mesh resolution did not have a significant effect on any of the CFD results. The mesh was refined systematically until a stable pressure drop across the filter was observed, and the redevelopment length from the inlet was compared to a correlation in the literature. An example of this process is described in Subsection 3.2.1. Pressure drop was chosen to investigate mesh independence as it is the parameter that is to be compared with experimental data. Sensitivity of the mesh to flow development was chosen as changes in the flow leads to varying results depending on the porous zone configuration.

3. Results and discussion

This section presents the experimental results, detailing the relationship between melt throughput and pressure drop across screen filters. Several porous zone configurations are then trialed to find good agreement with the experimental results. It also presents a discussion on why the different configurations give different results.

3.1. Experimental results

Fig. 4 shows pressure at the pressure transducer, shown in Fig. 2, found at each throughput interval. Pressure is given in psi, where 1 psi = 6894.76 Pa. Error was calculated by calculating standard deviation over the averaged pressure data, and was found to be universally under 2 psi, which would not be identifiable in Fig. 4. As expected, the pressure increases with increasing throughput and filter fineness. Pressure does not increase linearly with throughput.

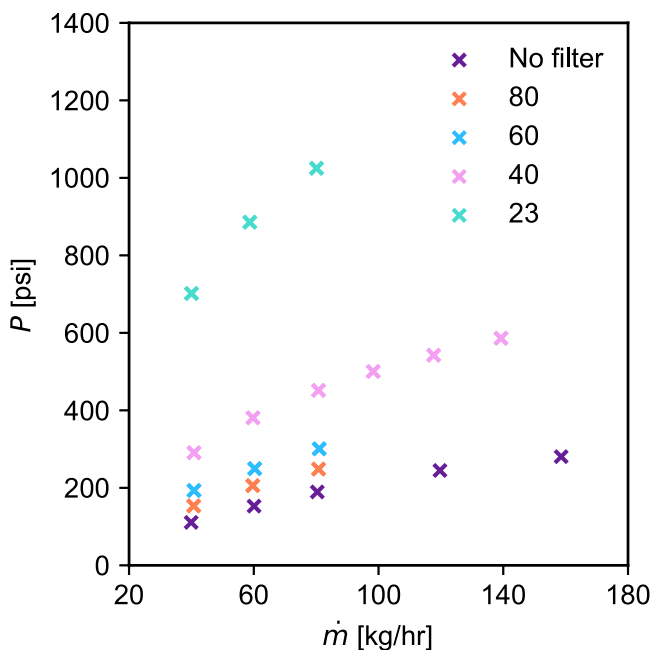


Fig. 4. Pressure against throughput for each filter.

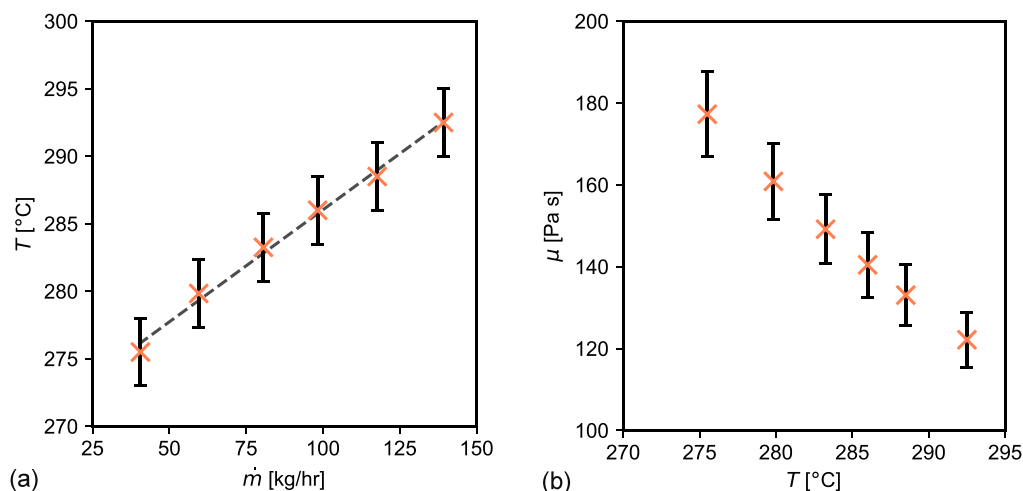


Fig. 5. (a) The average temperature recorded using the pyrometer at each throughput interval. (b) The relationship between melt viscosity and the temperatures recorded in (a), calculated from (6).

This can be explained by Fig. 5a, which shows the average temperature recorded using the pyrometer at the throughputs of interest. The temperature was found to vary by several degrees along the curtain, giving a range of 5 °C from one end of the curtain to the other. As a result, temperature was measured in the middle of the curtain, and this variation was accounted for with a ± 2.5 °C error. The temperature increased by nearly 20 °C over the range of throughputs. As throughput increases, the speed of the extruder screw increases, leading to an increase of shearing of the polymer melt, thus energy dissipates through heat. Increasing temperature leads to a decrease in viscosity, decreasing pressure drop.

Fig. 5b shows that over the range of temperatures recorded, the shear viscosity of the polymer varies by 38%. The relationship between shear viscosity and temperature was based on well established relationships that have been previously employed and validated in Champion (2015), Champion et al. (2015). The relationship is given as

$$\mu = 0.1 \left[10^{(2953/T - 2.1337)} \right], \quad (6)$$

where T is the temperature of the melt. The viscosity of polymer melts vary with temperature in an exponential manner (Vlachopoulos and Strutt, 2012). The Vogel–Fulcher–Tammann equation is of the same form as (6) and is frequently used to describe the temperature dependence on viscosity for polymer melts (Ikeda and Aniya, 2013). Wang Roger Porter et al. (1995) also highlight two of the most commonly used equations for expressing viscosity-temperature behaviour of polymer melts. One is an Arrhenius type equation and the second is the WLF equation (Wang Roger Porter et al., 1995), both express the relationship as an exponential decay in viscosity with increasing temperature.

The relationship between mass flow rate and pressure drop across the filter is of interest as this will clarify the physical behaviour of the melt. As the flow in the geometry is in the laminar regime and $Re < 1$, a Newtonian fluid would follow Darcy's law. Pressure drop across the filter therefore increases linearly with increasing mass flow rate. However, Fig. 5b shows that viscosity changes significantly over the range of flow rates used in the experiment. If this change in viscosity is not accounted for, the relationship between pressure drop across the filter and mass flow rate could not be established. To account for viscosity varying with temperature, a new variable, the corrected pressure ξ , is defined such that

$$\xi = P/\mu. \quad (7)$$

For each throughput in Fig. 4, an associated temperature was calculated from the line of best fit in Fig. 5a. This temperature was then used

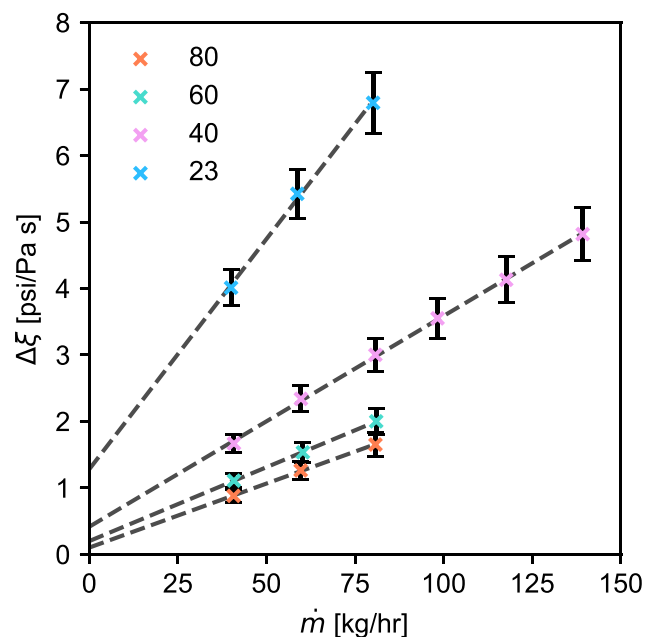


Fig. 6. Corrected pressure drop through each filter against throughput.

to find the viscosity and calculate ξ using the temperature-viscosity relationship.

Pressure drop across a filter can be determined at a particular throughput by subtracting the pressure reading of the system without a filter from the pressure reading of the system with a filter. Then, to obtain the pressure drop, a line of best fit was created for the no filter case for the pressure-throughput relationship. This gives the predicted pressure output through the system without a filter. This predicted pressure output was then subtracted from the pressure output obtained when the filter is in place to determine the pressure drop across the filter at that specific throughput.

From Darcy's law, dividing by viscosity,

$$\Delta\xi = \Delta P/\mu = (d/kA\rho)\dot{m}, \quad (8)$$

where A is the cross-sectional area of the filter, \dot{m} is the throughput and $\Delta\xi$ is the corrected pressure drop across the filter. That is, corrected pressure drop increases linearly with throughput in Darcy's regime.

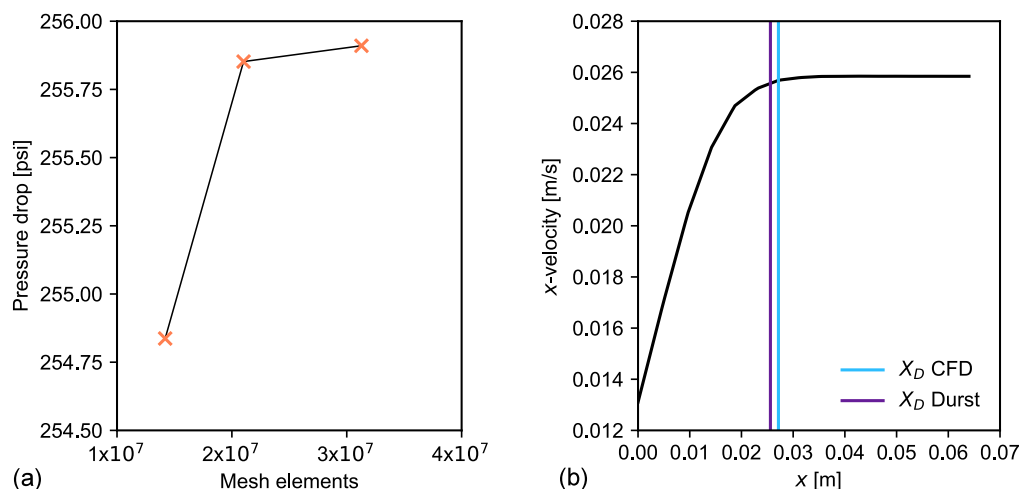


Fig. 7. (a) Pressure drop against number of mesh elements and (b) x -velocity along the centreline for the 80 μm filter in the filter away from holder case at a throughput of 80 kg/hr.

From Fig. 6, it appears that corrected pressure drop does indeed increase linearly with throughput. As accounting for temperature in the melt's viscosity recovers Darcy's law, the viscosity varies negligibly with shear rate; its zero shear viscosity limit applies throughout the experiment. Furthermore, as Darcy's law applies, the viscoelastic properties of this polymer melt are demonstrated to have a negligible effect on its flow through a screen filter.

From Fig. 6, the lines of best fit for each filter do not intercept the origin. As the filter grade reduces, thus the permeability of the filter decreases, the intercept increases. The shift may be due to non-linear effects at low throughputs, implying pre-Darcy behaviour, where the throughput-pressure drop relationship becomes nonlinear due to factors such as boundary layer effects (Diwu et al., 2018). Teng et al. (2024) present a comprehensive review on the literature investigating the pre-Darcy regime.

Temperature variations through the filter may also contribute to the shift. The shift may also be due to complex viscoelastic, non-Newtonian behaviour at low strain rates. As operating throughput decreases, the rate of strain imposed on the melt by the filter decreases. The melt viscosity-rate of strain relationship in porous media shows melt viscosity decreasing with strain rate, with several plateaus (Sochi, 2010). Experimental conditions may impose a range of strain rates on the melt such that the relationship remains in the intermediate plateau. Hence rate of strain would have no influence on melt viscosity throughout experimental conditions. Low operating mass flow rates may then increase melt viscosity due to a decrease in the strain rate imposed by the filter on the melt, resulting in non-linearity for the pressure drop-mass flow rate relationship.

Darcy's law has therefore only been shown to be valid over the range of flow rates shown for the experimental data in Fig. 6. The exact nature of the pressure drop and mass flow rate relationship as mass flow rates approach zero is beyond the scope of this work since it is outside of the operating regime of any practical applications that we are aware of. Nevertheless, it may be of scientific interest to investigate more thoroughly in future work.

3.2. Computational results

As Darcy's law (2) applies over the range of the experiment, permeability values for each filter grade can be calculated by obtaining the gradient from lines of best fit in Fig. 6. That is, using

$$k = \frac{d}{A\rho} \frac{1}{m_x}, \quad (9)$$

where m_x is the gradient from the line of best fit of an individual filter grade.

Fig. 3 highlights the screen filter structure, with the thickness of the downstream support mesh, the filter layer and the upstream support mesh prescribed d_D , d_F and d_U respectively. These thicknesses vary between filter grade, and were measured for each filter using a caliper. The total thickness of, for example, the 80 μm filter is therefore given by $d_{\text{total}}^{80} = d_U^{80} + d_F^{80} + d_D^{80}$, where the superscript represents the filter grade. For the 23 μm filter, which is made up of five total layers, d_{total}^{23} was taken as the sum of the two downstream support meshes and d_F^{23} was taken as the sum of the filter layer and the support mesh between the filter layer and the upstream support mesh. With this structure, three different porous zone configurations were tested to determine the most reliable configuration for predicting pressure drop across a multi-layered woven screen with CFD using the porous media model:

1. The "full length" model. The porous zone, for each filter grade, was prescribed a thickness of $d_{\text{total}} = d_U + d_F + d_D$ and it was placed directly against the filter holder. If this model gives good agreement with the experimental results, then the layers need not be considered, and a single permeability value can be successfully used to predict pressure drop across the multi-layer configuration of a screen filter.
2. The "filter by holder" model. Zero thickness was chosen for d_U and d_D , leaving the porous zone with a thickness d_F and placing it directly against the filter holder. If this model gives good agreement with the experimental results, then only the filter layer need be considered to successfully predict pressure drop across a screen filter.
3. The "filter away from holder" model. The porous zone was enabled only in d_F , placing the porous zone a distance d_D away from the filter holder. If this model gives good agreement with the experimental results, then only the filter layer need be considered when calculating permeability, but the position of the layer must be considered to successfully predict pressure drop across a screen filter.

For each of the porous zone configurations, the permeability of each filter grade was calculated from (9). Simulations were then run to match the targeted throughputs in the experiment. For example, for the 80 μm filter using the full length model, a mesh was created with a porous zone of thickness d_{total}^{80} . This was ensured to match the total measured thickness of the actual 80 μm screen filter. A permeability was then calculated from (9) using $d = d_{\text{total}}^{80}$, which was then prescribed to the porous zone. Then simulations were run at 40, 60 and 80 kg/hr to match the throughput intervals targeted by the experimental work. Simulations were also run with no porous zone prescribed to the geometry at throughputs in intervals of 20 kg/hr between 40–140 kg/hr.

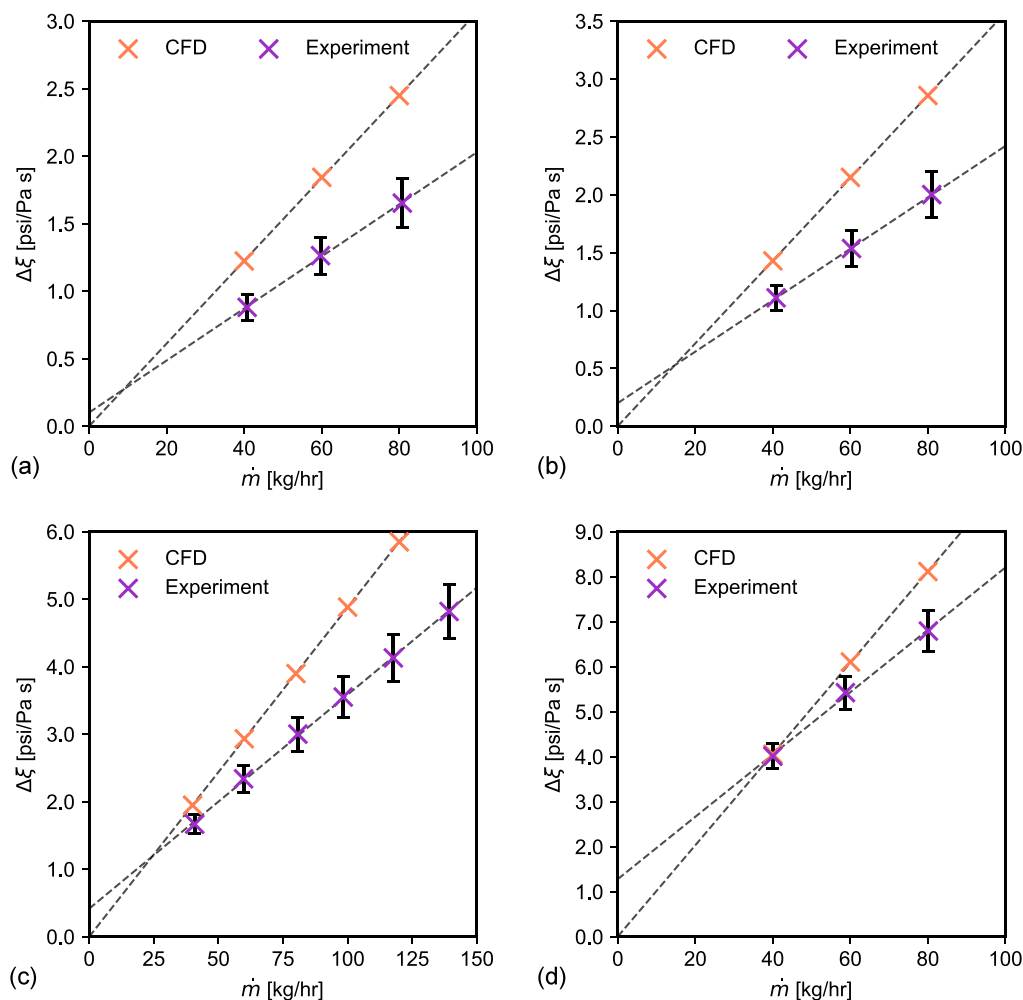


Fig. 8. Corrected pressure drop through (a) 80 (b) 60 (c) 40 (d) 23 μm filter against throughput from experimental data and the full length model. It may be observed that the full length model yields poor predictions.

Corrected pressure drop across the filter at each throughput was then calculated by subtracting the corrected pressure output from the no porous zone case away from the corrected pressure with the porous zone enabled.

3.2.1. Mesh independence study

For each unique geometry, three meshes were generated. All meshes were generated with tetrahedra cell shapes, with curvature capture specified to ensure sufficient mesh resolution in regions of significant changes in curvature. Fig. 7a shows the pressure drop output for the three meshes generated for the 80 μm filter in the filter away from holder case at a throughput of 80 kg/hr. There is shown to be less than a 0.025% change between the medium and fine mesh. Results were therefore deemed to be independent of choice of medium or fine mesh.

To further check the suitability of the medium mesh, the flow development length downstream of the filter holder was compared to the analytical relationship developed by Durst et al. (2005). This particular correlation is chosen as it accounts for the role diffusion plays in flow redevelopment in the creeping flow limit (Poole and Ridley, 2007). The relationship is given by

$$X_D/D = \left[0.619\text{Re}^{1.6} + (0.0567\text{Re})^{1.6} \right]^{0.625}, \quad (10)$$

where Re is the Reynolds number in the pipe, D is the pipe diameter and X_D is the development length. Fig. 7b shows a plot of x -velocity along the centreline of the pipe, starting from the inlet. The development length in the CFD model was determined by analysing the

x -velocity, pinpointing the point at which its variation along the length of the pipe is 0 m/s, to 4 decimal places. It is found to be in good agreement with (10), with a percentage error of under 5%. The medium mesh was deemed suitable to proceed with analysis.

Fig. 7b shows that the flow is fully developed before entering the filter system. This verifies that the inlet pipe was significantly long enough to fully develop the flow before entering the filter system, negating any influence of artificial boundary effects on the flow through the filter system.

3.2.2. Computational validation

Fig. 8 provides a comparison between the CFD results obtained using the full length model and the corresponding experimental data. The CFD model has been successful in capturing the linear relationship between throughput and pressure drop. However, it is apparent that there is poor agreement between experimental data and the full length model. It is worth noting that the full length model predicts a corrected pressure drop of 0 psi/Pa s at a throughput 0 kg/hr, which, as discussed, is not observed in the experimental data. This is a feature of a porous zone, as it is implementing Darcy's law. Thus, to compare the two, it is essential to focus on the gradients obtained from the CFD model and experimental data. It is found that there is around a 50% discrepancy in results. This poor agreement is because the full length model does not account for the multi-layered structure of the screen filters. Superior agreement is found when the different layers are accounted for.

Fig. 9 provides a comparison between the CFD results obtained using the filter by holder model and the corresponding experimental

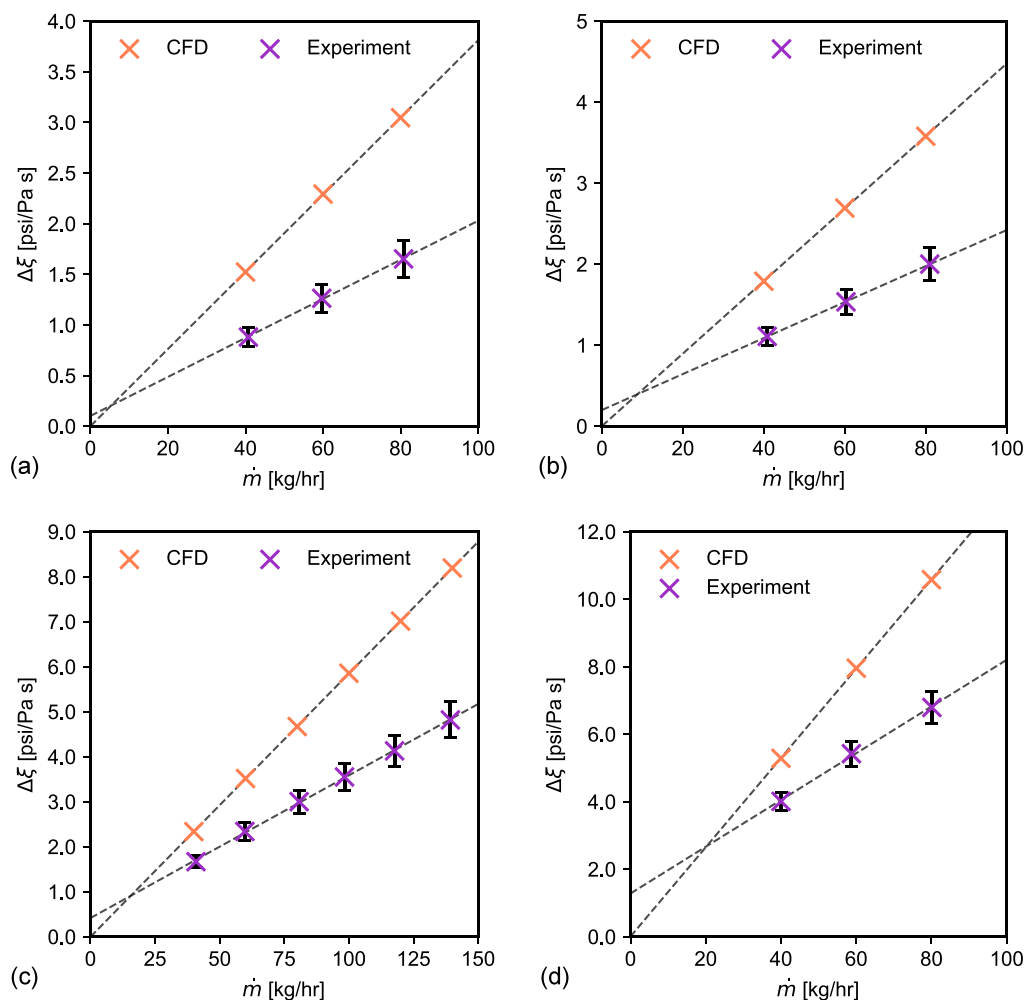


Fig. 9. Corrected pressure drop through a (a) 80 (b) 60 (c) 40 (d) 23 μm filter against throughput from experimental data and the filter by holder model. It may be observed that the filter by holder model yields poor predictions.

data. The filter by holder model has also been successful in capturing the linear relationship between throughput and pressure drop. However, it can be seen that the discrepancy in gradients between the filter by holder model and the experiments is even worse than the full length model. CFD predictions are off by around 100%. This suggests that position of the porous zone, relative to the filter holder, must be accounted for.

In Fig. 10, a comparison is presented between the CFD results obtained using the filter away from holder model and the corresponding experimental data. The filter away from holder model has been successful in capturing the linear relationship between the throughput and pressure drop. In all cases, the gradient error is under 5%, indicating good agreement between the experiment and CFD model. This suggests that only the filter layer needs to be represented by a porous zone, but for good agreement, it must be placed in its correct position relative to the filter holder, hence the thickness of the downstream support mesh is needed.

3.3. Discussion

The away from holder model produces results that are by far in best agreement with the experiment because the multi-layered configuration of the filter is accounted for through the thickness of the porous zone and its position relative to the filter holder. The filter medium itself

is far less permeable than the support layers, thus the pressure drop caused by flow resistance through the filter layer dominates the pressure drop through the screen filter. However, it is clear that the position of the porous zone relative to the filter holder influences results. By placing the porous medium the distance of the downstream support layer away from the filter holder, agreement with the experiment is superior.

Fig. 11 shows the x -velocity profile upstream of the porous zone for each model. As model accuracy compared to experimental results improves, there is a decrease in fluctuations in x -velocity upstream of the porous zone. This shows that by placing the porous zone a distance away from the holder, the resistance caused by the porous zone has a larger influence on the flow profile. As the porous zone is defined as isotropic and homogeneous, the flow redistributes so that velocity is constant across it. In pipe flow, as flow approaches an isotropic, homogeneous screen, it causes resistance to the flow, flattening the velocity profile (Abou-Hweij and Azizi, 2020). This flattening is most apparent in the filter away from holder model. The flattening is less apparent in the filter by holder and full length models, where the x -velocity profile has a similar shape to the no filter case. As the porous zone is in contact with the holder, the flow distributes to follow the path of least resistance through both the porous zone and the holder.

This is further verified by Fig. 12. In Fig. 12a, where no filter is inserted, flow is evenly distributed through each channel of the filter

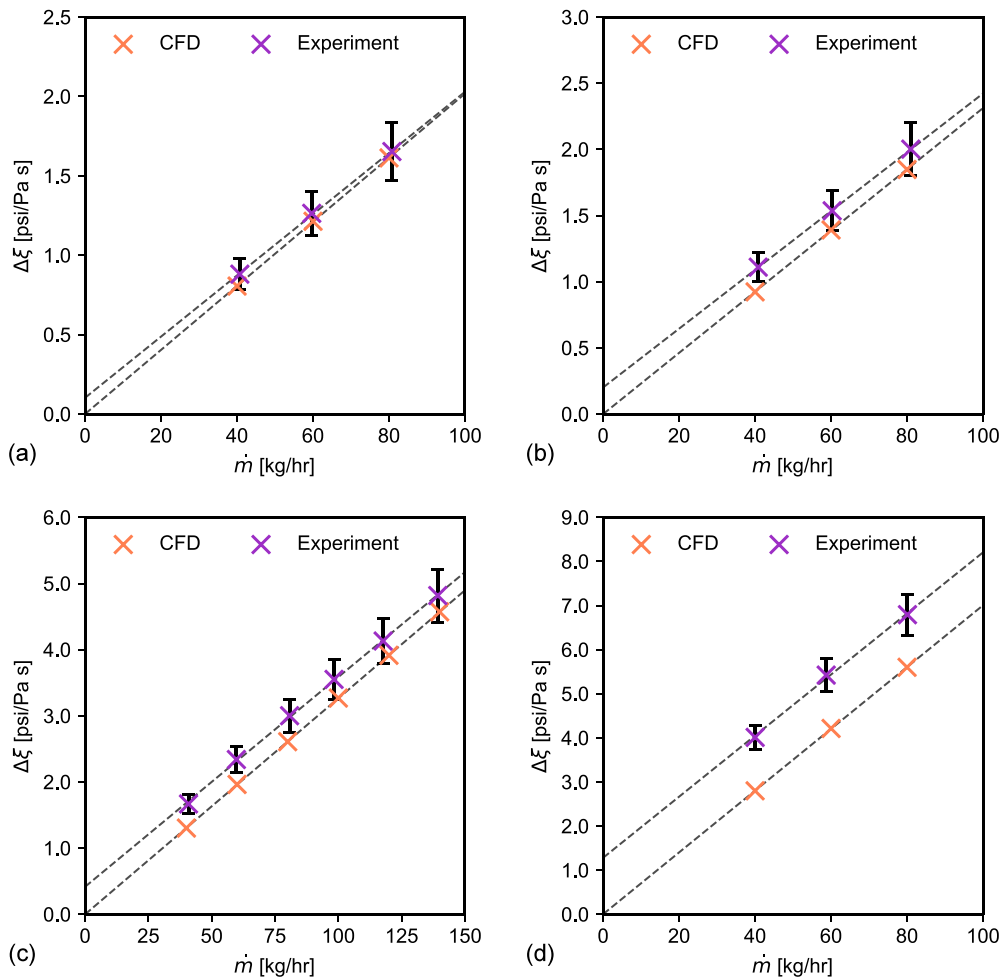


Fig. 10. Corrected pressure drop through a (a) 80 (b) 60 (c) 40 (d) 23 μm filter against throughput from experimental data and the filter away from holder model. It may be observed that the filter away from holder model yields very good predictions.

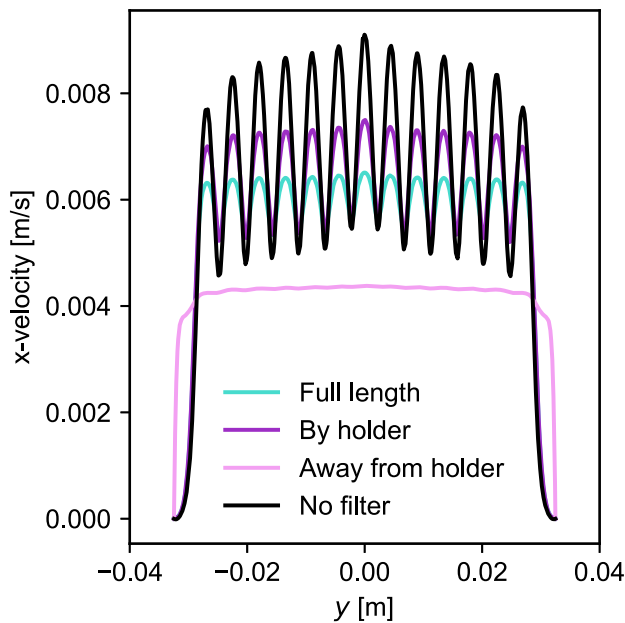


Fig. 11. Plot of x -velocity along y , 1.5 mm upstream of the holder for a no filter case, the full length model ($d_{\text{total}} = 0.9$ mm), the filter by holder model ($d_F = 0.12$ mm) and the filter away from holder model ($d_F = 0.12$ mm, $d_D = 0.55$ mm). All models have a throughput of 60 kg/hr. A 60 μm filter is modelled.

holder. In Fig. 12b, in the filter by holder model, the flow patterns closely resemble those observed in the absence of a filter; the distribution of flow remains well-balanced across each channel. Fig. 12c shows that, for the filter away from holder model, as the velocity is nearly constant across the porous zone, the majority of the flow most travel through the outer holes, due to the proportion of fluid in their vicinity. Overall, the filter away from holder model resolves the changes in flow as the melt moves between screen layers and the holder, whereas the other models do not.

The choice of filter grade employed is crucial in optimizing the film casting process. A lower grade filter ensures smaller contaminants are captured compared to a higher grade filter. However, Fig. 6 shows that decreasing filter grade results in a larger pressure drop penalty across the filter. This means that more energy is required for the melt pump to maintain a desired flow rate. It is therefore important to choose a filter grade which will not affect the quality of the final product while minimizing pressure drop across the filter to optimize cost-effectiveness of the process.

4. Conclusion

An experimental set-up, designed to investigate how pressure drop changed based on changes to melt throughput and filter permeability, was carried out. A computational model, using a porous zone to represent the screen filter, was created to model experimental results. Variations in porous zone length and position, based on the structure of a screen filter, were tested to see what configuration leads to the best agreement with experimental results.

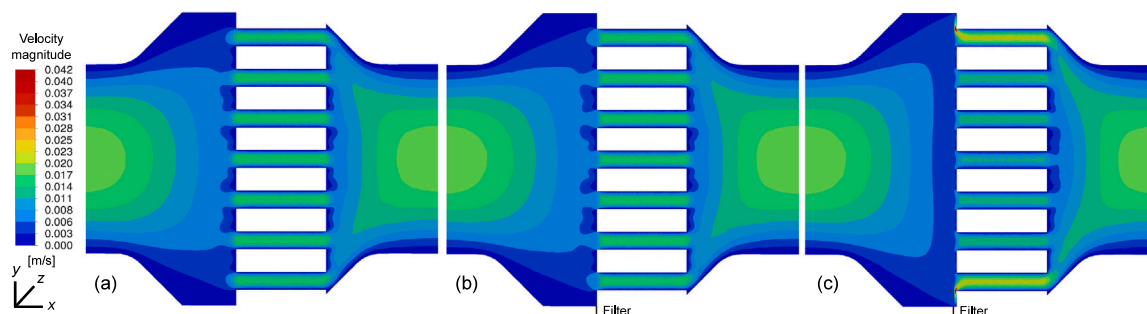


Fig. 12. Contours of velocity magnitude perpendicular to the holder for (a) a no filter case, (b) the filter by holder model and (c) the filter away from holder model. All models have a throughput of 60 kg/hr; (b) and (c) model a 60 μm filter.

Pressure drop was found to increase with decreasing filter permeability. Furthermore, corrected pressure drop, accounting for temperature variation, was found to increase linearly with increasing throughput for all filter grades at all throughputs investigated. This showed that over the range of the experiment, Darcy's law applied and PET melts act as a Newtonian fluids as they pass through screen filters.

It was found that to computationally model the pressure drop of a flow through a multi-layered woven screen, only the filtration layer needs to be modelled, but the presence of the downstream support layer needs to be accounted for. Using the sum of the screens as a thickness, or ignoring the support meshes completely, leads to inaccurate modelling. Instead, the filtration layer should be modelled with a porous zone, but placed correctly relative to the filter holder in the actual geometry. This allows for the correct capture of changes in flow distribution as the melt moves between screen layers and the holder. We emphasize that this conclusion, and the CFD methodology developed from it, is applicable to any CFD model of a filter system which utilizes a multi-layered screen filter, as long as the fluid is Newtonian and obeys Darcy's law across the screen filter.

CRedit authorship contribution statement

Joseph D. Bennett: Conceptualization, Formal analysis, Funding acquisition, Investigation, Methodology, Software, Validation, Visualization, Writing – original draft, Writing – review & editing. **Mark C.T. Wilson:** Conceptualization, Supervision, Writing – review & editing. **Nikil Kapur:** Conceptualization, Supervision. **Peter K. Jimack:** Conceptualization, Supervision, Writing – review & editing. **Richard P. Maltby:** Conceptualization, Investigation, Resources, Supervision, Writing – review & editing. **M. Kieran Looney:** Conceptualization, Investigation, Resources, Supervision, Writing – review & editing.

Declaration of competing interest

The authors declare no competing interests.

Data availability

Data supporting this study is openly available at doi: [10.17632/md487w94k2.1](https://doi.org/10.17632/md487w94k2.1).

Acknowledgements

This work was supported by the Engineering and Physical Sciences Research Council (EPSRC) Centre for Doctoral Training in Fluid Dynamics. This work was also supported by Mylar Specialty Films. For the purpose of open access, the author has applied a Creative Commons Attribution (CC BY) licence to any Author Accepted Manuscript version arising from this submission.

References

- Abou-Hweij, W., Azizi, F., 2020. CFD simulation of wall-bounded laminar flow through screens. Part I: Hydrodynamic characterization. *Eur. J. Mech. B Fluids* 84, 207–232. <http://dx.doi.org/10.1016/j.euromechflu.2020.06.008>.
- Ali, S.A., 2013. Design and evaluate a drum screen filter driven by undershot waterwheel for aquaculture recirculating systems. *Aquacul. Eng.* 54, 38–44. <http://dx.doi.org/10.1016/j.aquaeng.2012.10.006>.
- ANSYS, 2012b. ANSYS FLUENT 12.0 user's guide - 7.2.3 porous media conditions.
- Azizi, F., 2019. On the pressure drop of fluids through woven screen meshes. *Chem. Eng. Sci.* 207, 464–478. <http://dx.doi.org/10.1016/j.ces.2019.06.046>.
- Carley, J.F., Smith, W.C., 1978. Design and operation of screen packs. *Polym. Eng. Sci.* 18 (5), 408–415. <http://dx.doi.org/10.1002/pen.760180513>.
- Champion, J., 2015. Use of Computational Fluid Dynamics to improve the layer thickness control of polyester based multilayered films (Ph.D. thesis). University of Birmingham, Birmingham.
- Champion, J., Looney, M.K., Simmons, M.J., 2015. Numerical modeling of multilayer film coextrusion with experimental validation. *Polym. Eng. Sci.* 55 (8), 1829–1842. <http://dx.doi.org/10.1002/pen.24022>.
- Cornejo, I., Nikrityuk, P., Hayes, R.E., 2019. Pressure correction for automotive catalytic converters: A multi-zone permeability approach. *Chem. Eng. Res. Des.* 147, 232–243. <http://dx.doi.org/10.1016/j.cherd.2019.05.017>.
- Denn, M.M., 2008. *Polymer melt processing: foundations in fluid mechanics and heat transfer*. Cambridge University Press.
- Diwu, P., Liu, T., You, Z., Jiang, B., Zhou, J., 2018. Effect of low velocity non-Darcy flow on pressure response in shale and tight oil reservoirs. *Fuel* 216, 398–406.
- Durst, F., Ray, S., Ünsal, B., Bayoumi, O.A., 2005. The development lengths of laminar pipe and channel flows. *Transactions of the ASME* 127 (6), 1154–1160. <http://dx.doi.org/10.1115/1.2063088>.
- Garg, S.K., Premachandran, B., Singh, M., 2019. Numerical study of the regenerator for a miniature stirling cryocooler using the local thermal equilibrium (LTE) and the local thermal nonequilibrium (LTNE) models. *Therm. Sci. Eng. Prog.* 11, 150–161. <http://dx.doi.org/10.1016/j.tsep.2019.03.005>.
- Herman, M., 2004. In: Kroschwitz, J. (Ed.), third ed. *Encyclopedia of Polymer Science and Technology*, vol. 11, John Wiley & Sons, Inc., Hoboken, New Jersey, pp. 30–40.
- Ikeda, M., Aniya, M., 2013. Understanding the vogel-fulcher-tammann law in terms of the bond strength-coordination number fluctuation model. *J. Non-Cryst. Solids* 371–372, 53–57. <http://dx.doi.org/10.1016/j.jnoncrysol.2013.04.034>.
- Kołodziej, A., Jaroszyński, M., Janus, B., Kleszcz, T., Łojewska, J., Łojewski, T., 2009. An experimental study of the pressure drop in fluid flows through wire gauzes. *Chem. Eng. Commun.* 196 (8), 932–949. <http://dx.doi.org/10.1080/00986440902743851>.
- Laws, E., Livesey, J., 1978. Flow through screens. *Ann. Rev. Fluid. Mech.* 247–266.
- Omnexus, 2024. What are the main applications of PET? URL <https://omnexus.specialchem.com/>.
- Onufrena, A., Koettig, T., Dorau, T., Laguna, L., Bremer, J., Tirolien, T., ter Brake, H.J.M., 2021. Characterization of woven copper mesh as a heat transfer matrix at low temperatures. In: Ross, R., Raab, J., Miller, S. (Eds.), *International Cryocooler Conference, Inc.*, Boulder, pp. 413–422.
- Pachner, S., Aigner, M., Miethlinger, J., 2017. Modeling and optimization of melt filtration systems in polymer recycling. In: AIP Conf. Proc. 1914, American Institute of Physics Inc., pp. 1–5. <http://dx.doi.org/10.1063/1.5016744>.
- Pachner, S., Aigner, M., Miethlinger, J., 2019. A heuristic method for modeling the initial pressure drop in melt filtration using woven screens in polymer recycling. *Polym. Eng. Sci.* 59 (6), 1105–1113. <http://dx.doi.org/10.1002/pen.25088>.
- Pashchenko, D., Karpilov, I., Mustafin, R., 2020. Numerical calculation with experimental validation of pressure drop in a fixed-bed reactor filled with the porous elements. *AIChE J.* 66 (5), <http://dx.doi.org/10.1002/aic.16937>.
- Poole, R.J., Ridley, B.S., 2007. Development-length requirements for fully developed laminar pipe flow of inelastic non-Newtonian liquids. *Transactions of the ASME* 129 (10), 1281–1287. <http://dx.doi.org/10.1115/1.2776969>.

- P&S Intelligence, 2024. Polymer market share analysis by type (thermoplastics, thermosets, elastomers), base material (polyethylene, polypropylene, polyvinyl chloride, polyethylene terephthalate, polystyrene, polyurethane), application (packaging, construction, automotive, agriculture, electrical & electronics, textile) - global industry trends and growth forecast to 2030. URL <https://www.psmarketresearch.com/>.
- Sidiropoulou, M.G., Moutsopoulos, K.N., Tsihrintzis, V.A., 2007. Determination of forchheimer equation coefficients a and b. *Hydrol. Process.* 21 (4), 534–554. <http://dx.doi.org/10.1002/hyp.6264>.
- Sochi, T., 2010. Non-Newtonian flow in porous media. *Polymer* 51 (22), 5007–5023. <http://dx.doi.org/10.1016/j.polymer.2010.07.047>.
- Statista, 2024. Demand for polyethylene terephthalate worldwide from 2010 to 2020, with a forecast for 2021 to 2030. URL <https://www.statista.com/>.
- Stratiychuk-Dear, D., 2018. Enhancing product differentiation through direct extrusion addition (Ph.D. thesis). University of Birmingham, Birmingham.
- Teitel, M., 2010. Using computational fluid dynamics simulations to determine pressure drops on woven screens. *Biosyst. Eng.* 105 (2), 172–179. <http://dx.doi.org/10.1016/j.biosystemseng.2009.10.005>.
- Teitel, M., 2011. On the applicability of the Forchheimer equation in simulating flow through woven screens. *Biosyst. Eng.* 109 (2), 130–139. <http://dx.doi.org/10.1016/j.biosystemseng.2011.02.009>.
- Teng, Y., Li, Z., Chen, C., 2024. A comprehensive review of pre-Darcy flows in low-permeability porous media.
- Trilok, G., Srinivas, K.E.S., Harikrishnan, D., Gnanasekaran, N., Mobedi, M., 2022. Correlations and numerical modeling of stacked woven wire-mesh porous media for heat exchange applications. *Energies* 15 (7), <http://dx.doi.org/10.3390/en15072371>.
- Valli, A., Hyväluoma, J., Jäsberg, A., Koponen, A., Timonen, J., 2009. Pressure drop for low Reynolds-number flows through regular and random screens. *Transp. Porous Media* 80 (2), 193–208. <http://dx.doi.org/10.1007/s11242-009-9350-0>.
- Vlachopoulos, J., Strutt, D., 2012. The Role of Rheology in Polymer Extrusion. *Tech. rep, polydynamics*.
- Wang, Y., Yang, G., Huang, Y., Huang, Y., Zhuan, R., Wu, J., 2021. Analytical model of flow-through-screen pressure drop for metal wire screens considering the effects of pore structures. *Chem. Eng. Sci.* 229, <http://dx.doi.org/10.1016/j.ces.2020.116037>.
- Wang Roger Porter, J.-s.S., Wang, J., Porter, R.S., 1995. On the viscosity-temperature behavior of polymer melts. *Rheol. Acta* 34, 496–503.
- Yangpeng, L., Guoqiang, X., Luo, X., Jiandong, M., Haiwang, L., 2015. Effect of porosity on flow behavior and heat transfer characteristics of sintered woven wire mesh structures. *Tech. rep, Beihang University, Beijing*.